Review Article

Noriyuki Unno* and Jun Taniguchi

3D nanofabrication using controlled-acceleration-voltage electron beam lithography with nanoimprinting technology

https://doi.org/10.1515/aot-2019-0004
Received January 8, 2019; accepted April 25, 2019; previously published online May 30, 2019

Abstract: Nanostructures have unique characteristics, such as large specific surface areas, that provide a wide range of engineering applications, such as electronics, optics, biotics, and thermal and fluid dynamics. They can be used to downsize many engineering products; therefore, new nanofabrication techniques are strongly needed to meet this demand. A simple fabrication process with high throughput is necessary for low-cost nanostructures. In recent years, three-dimensional (3D) nanostructures have attracted much attention because they dramatically opened up new fields for applications. However, conventional techniques for fabricating 3D nanostructures contain many complex processes, such as multiple patterning lithography, metal deposition, lift-off, etching, and chemical-mechanical polishing. This paper focuses on controlled-acceleration-voltage electron beam lithography (CAV-EBL), which can fabricate 3D nanostructures in one shot. The applications of 3D nanostructures are introduced, and the conventional 3D patterning technique is compared with CAV-EBL and various 3D patterning techniques using CAV-EBL with nanoimprinting technology. Finally, the outlook for next-generation devices that can be fabricated by CAV-EBL is presented.

Keywords: 3D patterning; electron beam lithography; nanoimprint; nanostructure; roll substrate.

***Corresponding author: Noriyuki Unno,** Department of Mechanical Engineering, Sanyo-Onoda City University, Daigaku-dori 1-1-1, Sanyo-Onoda, Yamaguchi 756-0884, Japan, e-mail: unno@rs.socu.ac.jp
Jun Taniguchi: Department of Applied Electronics, Tokyo University of Science, 6-3-1 Niijuku, Katsushika-ku, Tokyo 125-8585, Japan

www.degruyter.com/aot

1 Introduction

As various nanopatterning techniques used for the fabrication of semiconductor devices have progressed, the range of applications for nanopatterns has been widened, e.g. microelectromechanical systems, lab-on-a-chip, cell culture, holographic memory, antireflective surfaces, surfaces for drag reduction, and heat transfer enhancement. The patterning size on a silicon wafer used in recent years is approximately 300 mm in diameter, which is sufficient for some applications. Furthermore, three-dimensional (3D) patterns can be obtained by repeating the conventional manufacturing processes for semiconductors, such as lithography, metal deposition, lift-off, etching, and chemical-mechanical polishing (CMP). New functions are obtained when the 3D pattern can be fabricated. In Section 1, the applications of 3D nanostructures and how to fabricate them using conventional nanopatterning technologies are described. Then, the 3D nanostructure fabrication method using controlled-acceleration-voltage electron beam lithography (CAV-EBL) is introduced in Section 2, and their suitability for the duplication of 3D nanostructures using transfer methods with nanoimprinting technology are described in Section 3. Moreover, some achievements using the obtained 3D nanostructures are shown in Section 4, and the summary is presented in Section 5.

1.1 Applications of 3D nanostructures

1.1.1 Electronic applications

Conventional nanopatterning techniques were originally developed for manufacturing semiconductor devices. There is a famous prediction about dense integrated circuits (ICs), i.e. Moore's law, which states that the number of transistors in an IC chip doubles about every 18 months. The lithography roadmap released by the IEEE International Roadmap for Devices and Systems shows that a

minimum half pitch will be <10 nm (10^{-9} m) in 2027 [1]. In the fabrication processes for IC chips, a 3D patterning technique is commonly used: e.g. a dual damascene process [2] (Figure 1A). A typical IC chip includes multilayer wiring; the metal wires in the lower and upper layers are connected by holes. To reduce the connecting error (due to the positioning error of a wafer stage) between the upper and lower wires at this time, both the hole and upper wiring layer are fabricated simultaneously. Furthermore, some processes (e.g. electroplating and CMP) are carried out only one time, while a single damascene process must repeat the processes. Moreover, freestanding T-shaped gate structures are used for high electron mobility transistors (Figure 1B). To fabricate a T-shaped gate structure, the interlayer is dissolved after the deposition of metal on a 3D pattern. Conventionally, these structures are fabricated with a multilevel resist process [3–10]. However, the multilayer resist process requires two or more resists, and these must be spun coated on a substrate separately. Moreover, the dedicated developers for each resist layer are needed, resulting in a complicated and time-consuming process. To fabricate a 3D pattern with high throughput at low cost, a simple technique is strongly desired.

1.1.2 Optical applications

The wavelength of visible light is about 400–800 nm; therefore, visible light is affected by nanostructures. For example, a conical nanostructure array (called a moth-eye structure) is used as an antireflective coating (Figure 2A) [11]. To achieve a low reflective index, the pitch and height of the conical nanopattern should be less than the wavelength and above a few hundred nanometers, respectively. In the moth-eye structure, the effective refractive index is gradually changed from the index of air to that of the structured material. The antireflective coating using the moth-eye structure is superior to a multilayer interference coating because the moth-eye structure has a lower reflectance and higher resistance to oblique light irradiation.

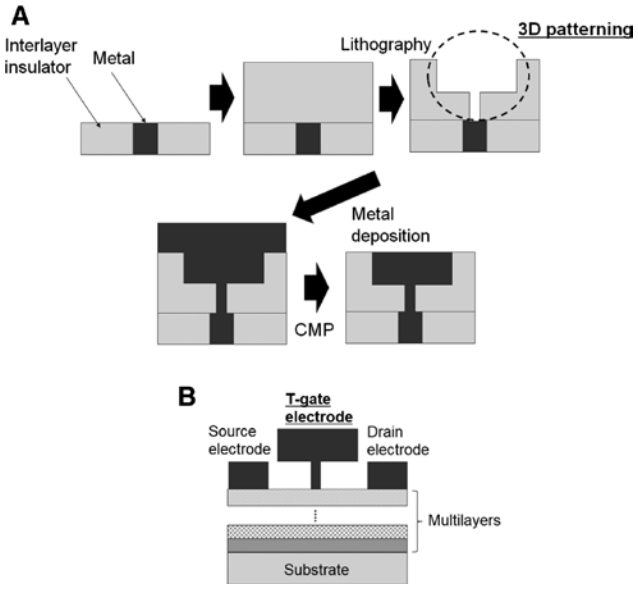

Figure 1: Schematic view of (A) the dual damascene process and (B) the T-gate structure where 3D nanopatterns are needed.

Computer-generated hologram read-only memory (CGH-ROM) is expected to be a next-generation optical recording medium (Figure 2B) [12]. CGH-ROM's reading speed and recording capacity are much higher than those of conventional optical memory. CGH-ROM consists of 3D nanostep patterns, whose vertical interval is <100 nm.

3D photonic crystals [13], which consist of periodic nanostructures in the x-y-z directions, are also attracting much attention because they can control optical propagation (Figure 2C). The photonic crystal is a promising technology for optical communication on chips.

1.1.3 Functional surface modifications

When nanostructures are fabricated on a surface, the surface properties can then be modified (Figure 3). For example, the surface wettability can be changed to superhydrophilic or superhydrophobic by fabricating the nanostructures on a surface. The lotus effect [14] is typically employed for fabricating a superhydrophobic surface used for self-cleaning [15] or antifrost coatings [16]. Moreover, the nanostructures inspired by cicada and dragonfly wings have been demonstrated as antibacterial surfaces [17, 18]. The rose petal effect [19] is also useful for the hanging-drop method [20], which can obtain spheroids, because the rose petal effect can produce a superhydrophobic state with high adhesive force.

1.1.4 Thermal and fluids engineering

3D hierarchical structures, which consist of both nano- and microstructures, are used for thermal and fluids engineering. For example, boiling heat transfer enhancement was demonstrated using the hierarchical structures made by the deep reactive ion etching technique and electroplating [21]. Critical heat flux can be improved using the hierarchical structures. In addition, nanostructures on microriblets are used for drag reduction in fluid flow [22].

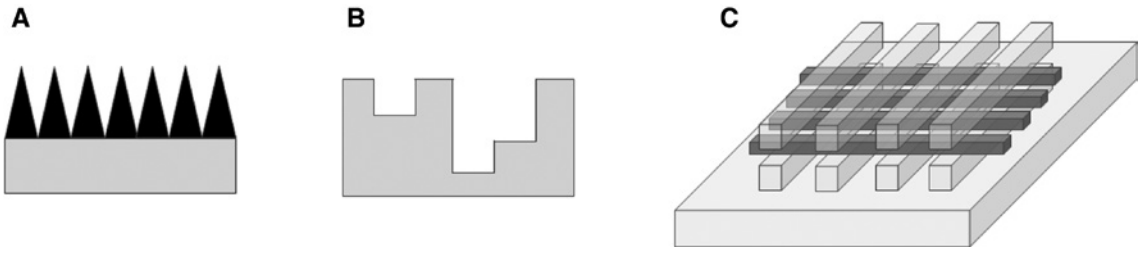

Figure 2: 3D nanopatterns used for optical applications: (A) moth-eye structure, (B) CGH-ROM pattern, and (C) 3D photonic-crystal structure.

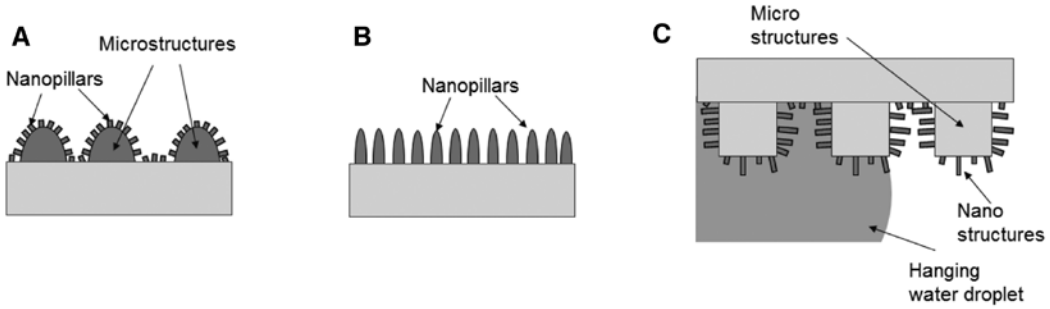

Figure 3: 3D nanopatterns used for surface modifications: (A) the lotus effect, (B) the cicada and dragonfly wings, and (C) the rose petal effect.

1.2 Conventional techniques for making 3D structures

1.2.1 Direct laser writing

Using a photopolymer, direct laser writing (DLW) [23] can be used in 3D structure fabrications (Figure 4). There are three types of the DLW method: the serial (Figure 4A), parallel (Figure 4B), and multi-photon polymerization methods (Figure 4C). The irradiated part of the resist is dissolved (called a positive-type resist) or remained (called a negative-type resist) after the development process. As a result, a 3D structure can be obtained after development. When the multi-photon polymerization method was used, in particular, the irradiated photon is nonlinearly absorbed in photopolymers, and the spot size of the photopolymerization area is <100 nm. The DLW process can be operated in air, and a vacuum chamber is not necessary. Moreover, 3D structures can be obtained with DLW when the DLW stage is moved in the x-y-z directions using a piezo stage. Galvanometer mirrors are also used for scanning laser beams in the serial method. In the case of 3D fabrication with DLW, the gray-tone lithography technique is used [24–26]. However, the resolution of a sub-micron pattern is challenging because of the spot size of the laser. On the other hand, <10-nm line patterns with a two-line resolution of 52 nm using the stimulated emission depletion method have been reported [27].

1.2.2 Electron and ion beam lithography

Electron and ion beams are also used for direct writing lithography (Figure 5). The spot size of electrons [28] or helium ion beams [29] is much smaller than that of the laser beam used in DLW (e.g. a diameter of a few nanometers is possible). Therefore, a <10-nm pattern is obtained using EBL. To obtain 3D structures using EBL, the multi-electron beam (EB) dose method is typically used [30, 31]. Ion beam milling is commonly used for cutting 3D structures. Because of their very high resolution, these techniques are used to fabricate photomask patterns or nanoimprint molds.

1.2.3 Energy beam-induced deposition

Energy beams are used not only for lithography or milling processes but also for deposition processes with ions [32] or EBs [33] generated in a vacuum condition. When a precursor gas injection system was installed in the vacuum chamber of the energy beam system, it is possible to

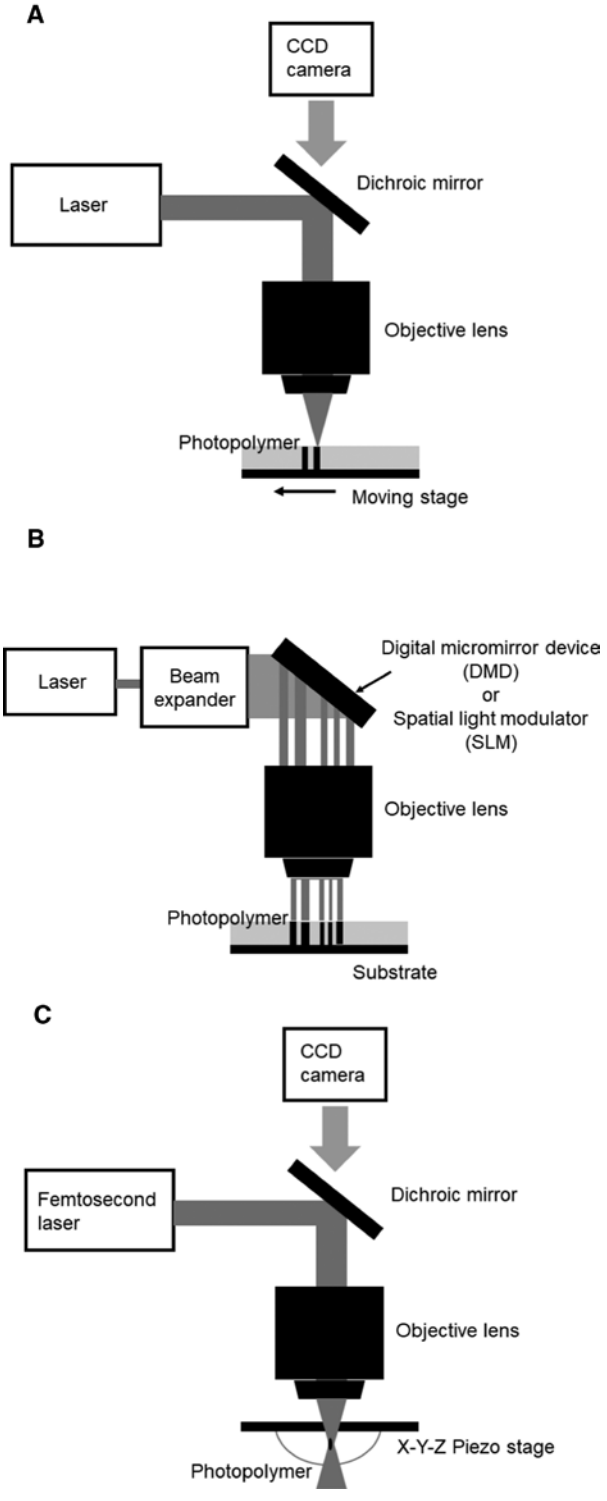

Figure 4: A typical experimental setup for DLW using (A) the serial method, (B) the parallel method, and (C) the multi-photon polymerization method.

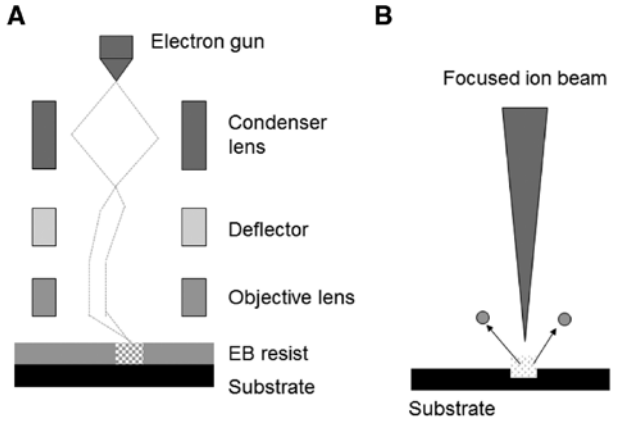

Figure 5: Schematic view of (A) EBL and (B) ion beam milling.

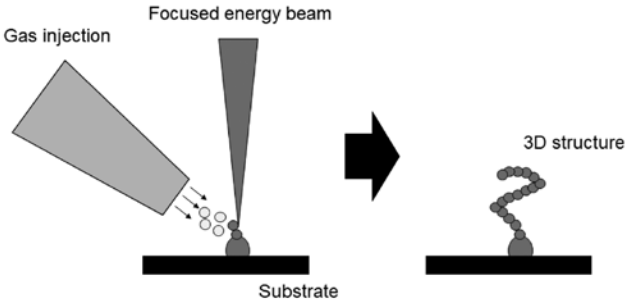

Figure 6: Schematic view of an electron beam-induced deposition process.

fabricate a 3D nanostructure (Figure 6). In this system, the precursor gas is affected by the energy beam and changes into nonvolatile and volatile compounds. The volatile compound is removed via a vacuum pump. Various metals and diamond-like carbon can be deposited by this process.

2 3D nanostructure mold fabrication using CAV-EBL

As noted in the previous section, various techniques to obtain 3D nanostructures have been reported. Some techniques have a high resolution of <10 nm, while other techniques have a high throughput. However, it is challenging to obtain 3D nanostructures in large areas with both high resolution and high throughput. A fine mold for nanoimprinting technology (e.g. <10-nm patterns are possible) can be obtained using EBL. However, the throughput of EBL is very low because it is a direct writing technique (e.g. several days are needed for writing). In contrast, despite its very high throughput, the resolution of the nanoimprinting technology depends on the mold pattern. Therefore, the combination of EBL with

nanoimprinting technology is a promising technique for meeting the demand. However, 3D nanostructure mold fabrication using EBL is challenging. EB dose time control is typically used for 3D patterning [34, 35]; however, it is difficult to obtain a fine 3D structure, especially <100 nm, by varying the dose time. CAV-EBL [36] has attracted much attention in fabricating fine 3D molds. In the following section, the CAV-EBL technique is described in detail.

2.1 The principle of CAV-EBL

In the EBL process, an EB resist is affected by irradiated electrons or secondary electrons. As a result, the irradiated part of the EB resist is dissolved (called a positive-type EB resist) or remained (called a negative-type EB resist) in the development process. When EBL is used for the fabrication of 3D structures, the EB dose time is typically varied while the EB acceleration voltage is kept constant (Figure 7A). With positive properties, in this case, a higher EB dose tends to fabricate a deeper pattern; thus, the depth of developed patterns can be controlled easily by varying the EB dose time. However, the electron irradiated to the EB resist is scattered in the EB resist or the substrate. These phenomena are called forward and back scattering, respectively. Therefore, the pattern width of the developed pattern tends to be wider with a higher EB dose, and it is difficult to obtain a <100-nm 3D pattern using EB dose time control.

In contrast, an EBL process that varies the EB acceleration voltage has the potential to fabricate <100-nm 3D structures (Figure 7B) [37]. This technique is called CAV-EBL [38]. The main advantage of CAV-EBL is its precise control of the developed depth (e.g. 5-nm steps with 30 V [38]). It is well known that the EB range depends on the EB acceleration voltage and the material properties of EB resist [39]. Therefore, the developed depth can be changed precisely by varying the EB acceleration voltage. Thus, the EB dose time can be optimized independently of the EB acceleration voltage. As a result, CAV-EBL can perform precise control of the pattern depth and width simultaneously.

When a negative-type EB resist is used for CAV-EBL, a midair structure can be obtained [40–42]. Figure 8 shows the schematic view of a CAV-EBL process for the fabrication of midair structures. First, hydrosilsesquioxane (HSQ), which is a negative-type EB resist, is coated on a substrate. After that, the beam and bridge parts are exposed to an EB accelerated by high and low voltages, respectively. On the one hand, at this time, the EB accelerated by a high voltage reaches the substrate under the EB resist layer. On the other hand, the penetration depth of an EB accelerated by a low voltage is controlled to be less than the thickness of the EB resist layer. With a negative-type EB resist, only the exposed area remained after the development and midair structures are consequently obtained. Figure 9 shows the midair structures fabricated by CAV-EBL. Here, an HSQ resist of 300-nm thickness on a silicon substrate was used. The acceleration voltages were 30 and 3 kV. Bridges formed between beams can stand in air freely. By using a 1-kV EB as the low-voltage EB, bridges with thickness of 100 nm were obtained [40]. SU-8 [43], which is a famous photo and EB resist, was used for this purpose [44]. The width of the obtained bridge made of SU-8 was above 1 μm.

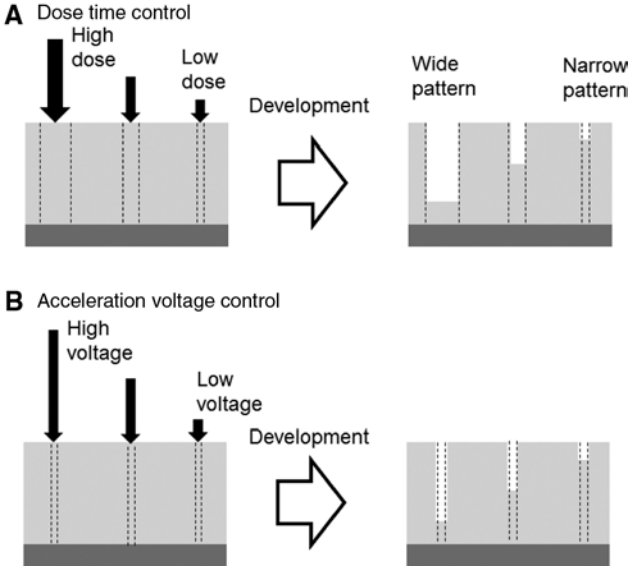

Figure 7: Fabrication techniques for 3D structures using EBL with positive resist behavior: (A) conventional dose time control and (B) CAV-EBL.

2.2 EB resists for CAV-EBL

Although CAV-EBL can be used with various EB resists, the EB acceleration voltage must be low when a shallow pattern is needed. It is well known that forward scattering [45, 46] is easily caused with a low EB acceleration voltage [47]. Thus, a higher-contrast EB resist is preferred to fabricate fine 3D structures using CAV-EBL [48]. If the developed pattern fabricated by CAV-EBL is possible to be used for nanoimprinting directly, there is no need to carry out complex processes such as metal

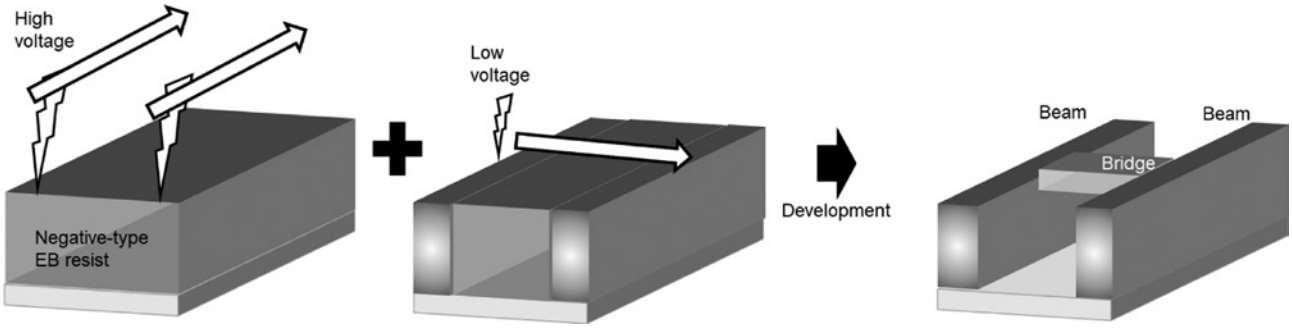

Figure 8: CAV-EBL process with a negative-type EB resist to fabricate midair structures with negative resist behavior.

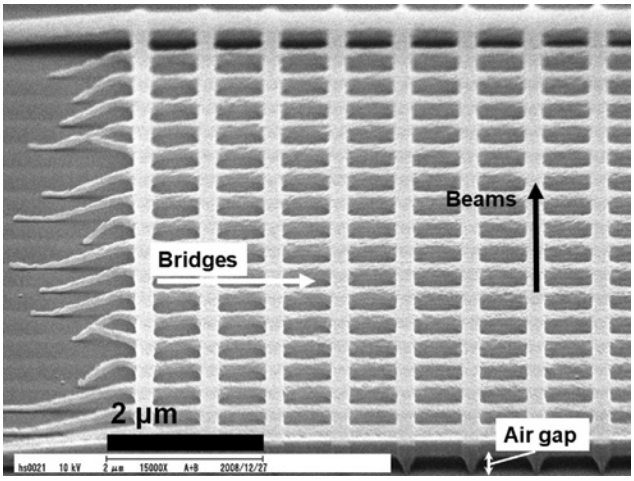

Figure 9: Tilted scanning electron microscopy images of the midair structures fabricated by CAV-EBL with an HSQ resist of 300-nm thickness.

deposition and dry etching. Therefore, a hard material is suitable for the combination process of CAV-EBL with nanoimprinting technology. In performing the combination of CAV-EBL with nanoimprinting without using complex processes, spin-on-glass (SOG) and HSQ are suitable EB resists. After spin coating and curing, the main component of SOG and HSQ is siloxane (the Si-O-Si linkage), which is hard and transparent. Furthermore, SOG and HSQ have high heat tolerance because the curing temperature for both SOG and HSQ is above 300°C. Thus, the 3D structures made from SOG or HSQ by CAV-EBL are suitable for use in nanoimprinting technology. Using SOG, for example, sub-100 nm line patterns can be obtained with the EB at 1–5 kV, while the pattern depths were ca. 50–200 nm [37]. Note that the pattern depth is restricted by the initial resist thickness and the penetration depth of electrons into an EB resist in principle.

2.3 Nanostep fabrication

Using an SOG as a positive-type EB resist, the fabrication of a nanostep is a typical application of CAV-EBL. As noted above, the developed depth can be controlled precisely with CAV-EBL. Figure 10 shows the atomic force microscopy (AFM) image of a typical nanostep pattern obtained by CAV-EBL with an SOG resist. The depth step is approximately 50 nm. The minimum step of the depth control is 5 nm with a 30-V step in the acceleration voltage [38]. In addition, it is possible to fabricate a <100-nm 3D line pattern using CAV-EBL [37].

2.4 Superresolution technique

SOG can be used as a positive-type EB resist, and it is not a chemically amplified resist (CAR). The postexposure bake (PEB) process is usually used with a CAR to enhance the

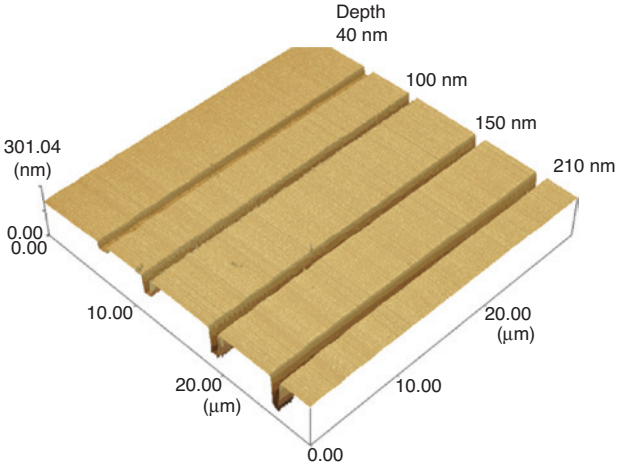

Figure 10: AFM image of the fabricated nanostep by CAV-EBL with an SOG resist.

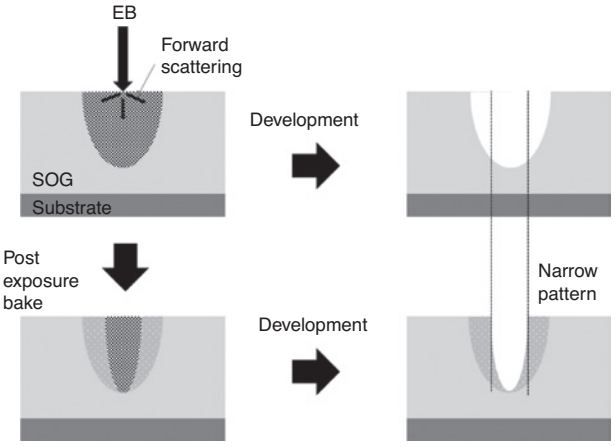

Figure 11: Schematic views of the effect of PEB on an SOG resist.

sensitivity. The PEB process is performed after EB exposure and before the development. Although SOG is not a CAR, a unique phenomenon is observed after the PEB process, i.e. superresolution [49–52]. Figure 11 illustrates the PEB effect on an SOG resist. In CAV-EBL, the EB acceleration voltage is lower than that in the conventional EBL. Therefore, backscattering can be ignorable. However, forward scattering is a problem in fabricating a narrow pattern because the scattered EB affects a large area of the SOG layer. In contrast, the PEB process makes the SOG layer exposed by the EB hard and decreases the etching rate in the developer. As a result, a narrower developed pattern can be obtained compared with no PEB process. Figure 12 shows the superresolution effect by PEB with an SOG layer. The obtained pattern at 100 μC/cm^2 without the PEB process is wider than that at 200 μC/cm^2 with the PEB process at 350°C. The PEB process reduces the proximity effect caused by forward scattering.

3 Transfer technique of 3D nanostructures from a mold obtained by CAV-EBL

Nanoimprinting technology, which utilizes a mold with nanopatterns, was developed in the 1990s. Recently, nanoimprinting was recognized as a promising technique for fabricating nanopatterns at very high throughput. There are two main nanoimprinting processes, i.e. thermal nanoimprint lithography (T-NIL) [53] and ultraviolet nanoimprint lithography (UV-NIL) [54] (Figure 13). Although a nanopatterned mold is necessary, the reversal pattern compared to the mold's pattern is duplicated to transferred substrates or films, resulting in a very high throughput. Reverse nanoimprint lithography is also attracting attention because it can stack nanostructures repeatedly using ultraviolet curable resins or thermoplastics [55–59].

For the further improvement of the throughput of nanoimprinting technology, roll-to-roll nanoimprint (RTR-NIL) is a promising technique [60]. A roll mold with 3D nanostructures is necessary for RTR-NIL. Figure 14 shows the typical setup system for RTR-NIL. When a seamless roll mold was obtained, continuous 3D structures could be duplicated in a large area. Therefore, a seamless patterning technique onto roll substrates is needed. Normal EBL and CAV-EBL processes using a roll substrate have been reported previously [61, 62]. Figure 15 shows the HSQ pattern on a quartz roll mold fabricated by EBL. In addition, the lift-off process is also possible on a roll substrate with the obtained pattern [63]. Because it is challenging to obtain a large roll mold using CAV-EBL because of the long writing time, a duplication technique from a small roll mold to a large roll

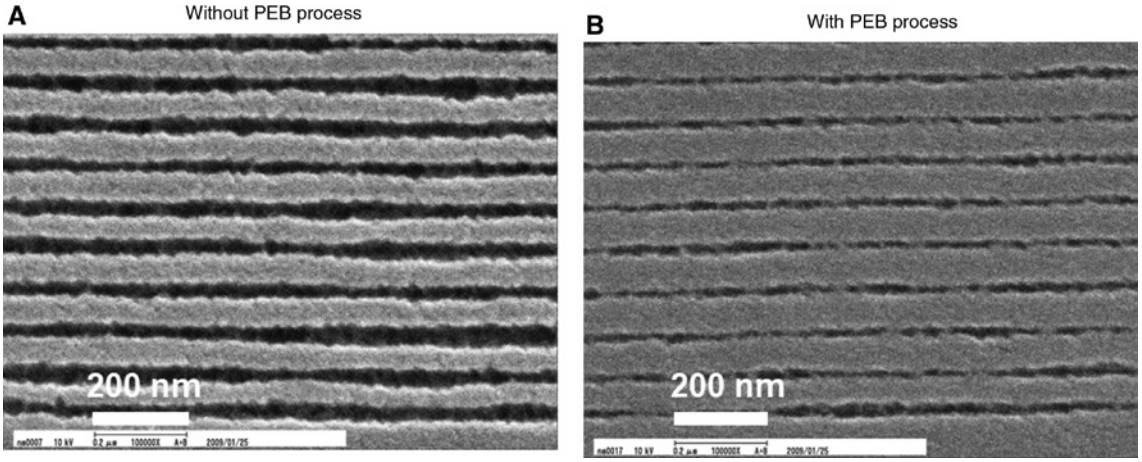

Figure 12: Superresolution technique using the PEB process for SOG: (A) without PEB and (B) with PEB at 350°C.

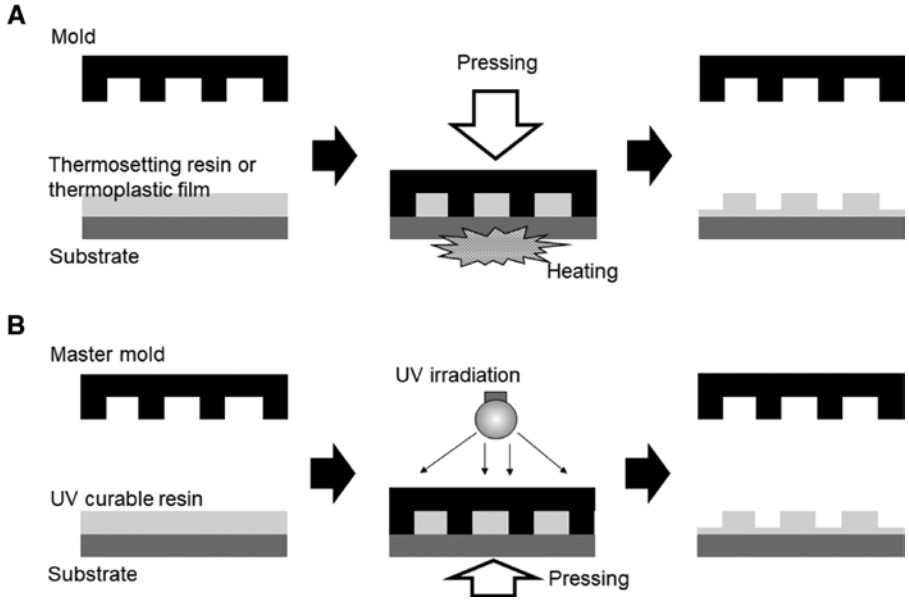

Figure 13: Typical nanoimprinting processes: (A) T-NIL and (B) UV-NIL.

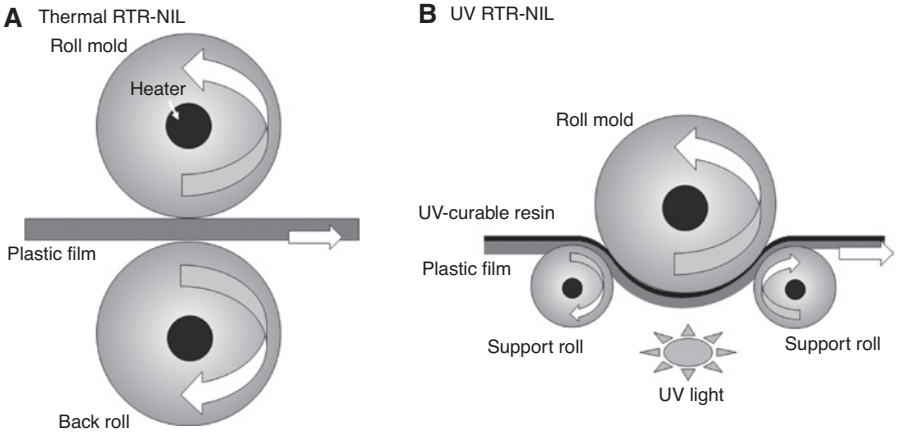

Figure 14: RTR-NIL with (A) thermoplastic film and (B) UV-curable resin.

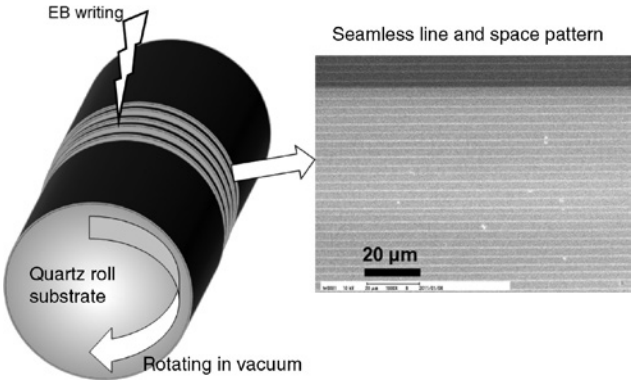

Figure 15: A seamless HSQ pattern fabricated on a quartz roll substrate.

mold was developed [64]. Moreover, the superresolution technique using the PEB process can be used for roll substrates [50].

CAV-EBL with SOG or HSQ is a powerful technique for fabricating 3D nanostructures. However, some applications require 3D nanostructures made of metals. Because it is difficult to obtain the metal 3D structures directly with the EBL technique, dry-etching processes are usually employed. To reduce the cost of the dry-etching machine and improve the productivity, nanotransfer printing (nTP) [65, 66] is a suitable technique for duplicating 3D nanostructures made of metals. Figure 16 illustrates the typical nTP process. At first, the

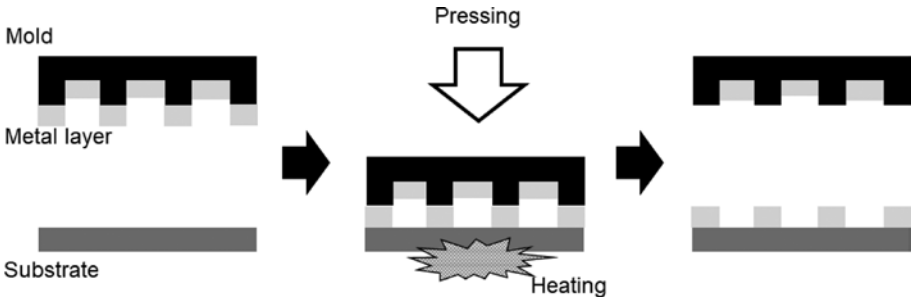

Figure 16: The nTP process for fabricating metal patterns.

nanopatterned mold is coated with a thin metal layer by a deposition method. Then, the transferred substrate is contacted with the mold while heating and pressing. Finally, the mold is released from the substrate after cooling, leaving the metal pattern on the substrate. The combination of the nTP process and 3D nanostructures obtained by CAV-EBL produces many progressive applications. In addition, metal 3D structures can be stacked repeatedly with the nTP process similar to reverse nanoimprint lithography [67, 68].

Figures 17 and 18 show the three main types of nTP processes using 3D nanostructures, i.e. (a) filling the mold with a metal layer [69], (b) a split metal layer [70], and (c) liquid adhesive filling [71]. Before the nTP processes, the obtained mold is coated with a thin chromium layer and oxidized. The obtained Cr_2O_3 layer improves

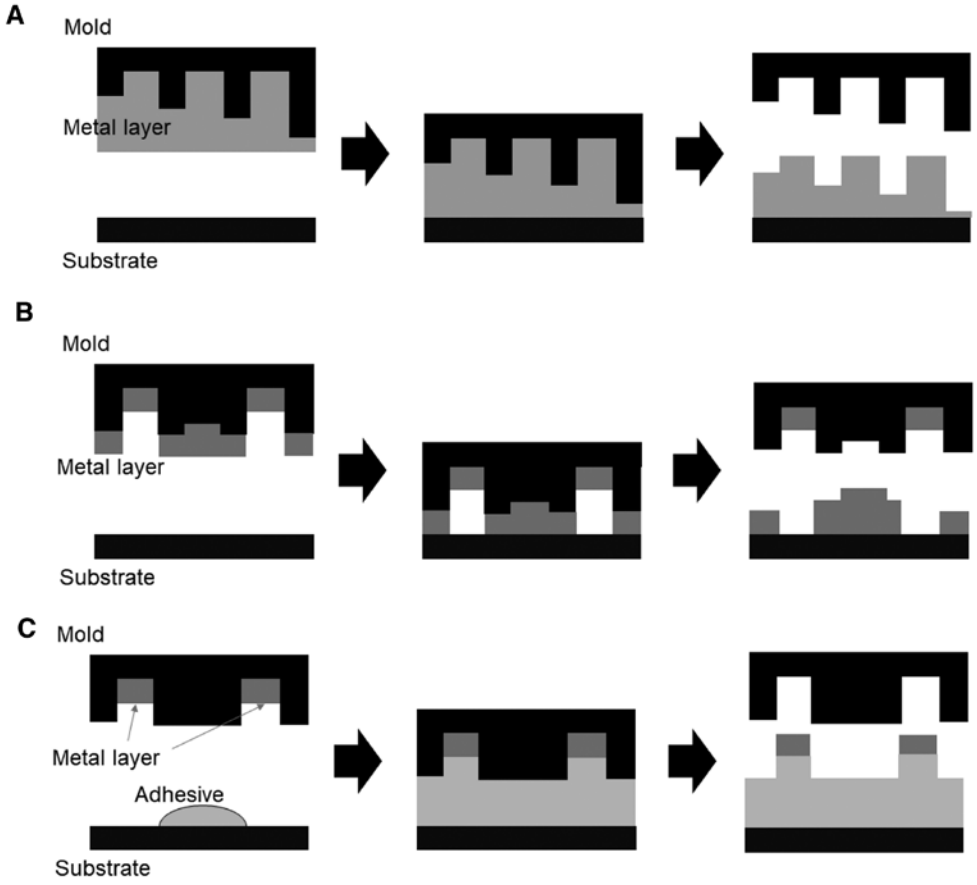

Figure 17: The nTP processes using 3D nanostructures: (A) filling the mold with a metal layer [69], (B) a split metal layer [70], and (C) a liquid adhesive filling [71].

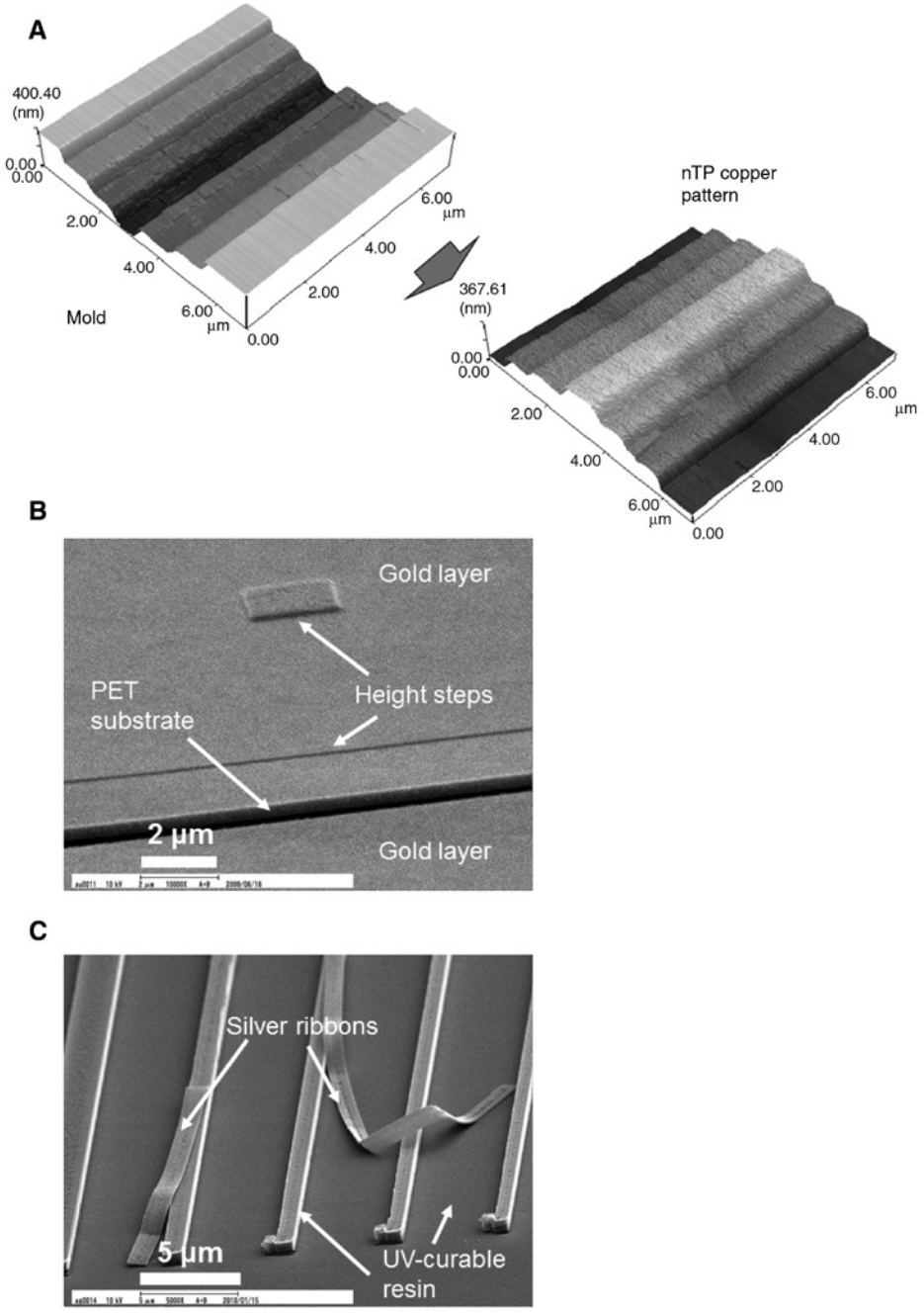

Figure 18: Demonstration of three types of nTP processes: (A) filling the mold with a metal layer, (B) a split metal layer, and (C) a liquid adhesive filling.

release property [66]. The nTP of filling the mold with a metal layer is the simplest process, and the deposited thickness of the metal layer is thicker than the height of the mold. The obtained pattern using the filling method is suitable for optical applications, e.g. binary blazed reflection gratings. The second method is to use a split metal layer. In this method, the metal layer in the deepest part of the mold is not transferred, which enables the design of isolated areas. Therefore, this method is potentially preferred by electronics applications. Additionally, the nTP process using a liquid adhesive is a very useful technique for obtaining metal dot patterns, which is used for plasmonic applications. Furthermore, a two-tone nTP process was also developed using a liquid adhesive [72]. Both UV-curable and thermosetting resins can be used for this purpose.

4 Applications of the 3D structures fabricated by CAV-EBL and nanoimprinting technology

The combination of CAV-EBL with nanoimprinting technology was introduced in the previous section as well as the supplementary techniques for CAV-EBL. In this section, some possible applications using these techniques are pointed out.

4.1 CGH-ROM

CAV-EBL will be very useful for the fabrication of CGH-ROM because it consists of nanosteps. Figure 19 shows the AFM images of a part of the CGH-ROM pattern obtained by EBL using the PEB process. The size of one dot area is <500 nm; thus, the superresolution technique using the PEB process is employed. There are four nanosteps, and the edge of the pattern is sharp and smooth. When this pattern was fabricated by the repetition of EBL and dry etching, a positioning system with very high quality (i.e. high cost) would be needed. In contrast, with the use of EBL with the PEB process, there is no need to align the sample and repeat the lithography process, including spin coating, baking, and development. The reconstruction results and further information were described previously [73–75]. Although the normal EBL was used here, 16 steps will be needed to improve the diffraction efficiency in the future, and CAV-EBL will be a promising technique. Therefore, the fabrication of optical elements including the CGH-ROM is one of the desirable applications using CAV-EBL.

4.2 3D metal electrode fabrication on plastic substrates for printed electronics

Printed electronics (PE) on plastic substrates attracts much attention because plastic substrates offer flexibility, lightness, low cost and transparency and are eco-friendly. As the conventional silicon transistors have been improved by shrinking the pattern size, the transistor on PE devices also needed to become smaller. Therefore, a 3D metal electrode is needed to fabricate complex patterns in PE devices. To meet the demand, the combination of CAV-EBL and nTP will be a powerful technique. Figure 20 shows the fabricated 3D metal electrode pattern with CAV-EBL and nTP of the split metal layer. There are three contact pads with 3D tips in the center. The electrical property of the transferred pattern has been reported previously [76], and a <50-nm gap can be obtained by nTP [66]. A roll mold can also be used in performing nTP [77].

4.3 Calibration plate for total internal reflection fluorescence microscopy with refractive index matching

Total internal reflection fluorescence microscopy (TIRFM) is a promising technique to measure the x-y-z fluid flow in nanoscale channels [78, 79]. To measure the fluid flow via TIRFM, the intensity calibration of a fluorescent particle is necessary using calibration plates, which have nanosteps. The most important point is that the surface of the glass substrate must be uncovered. The conventional nanoimprinting process has the problem of residual layer

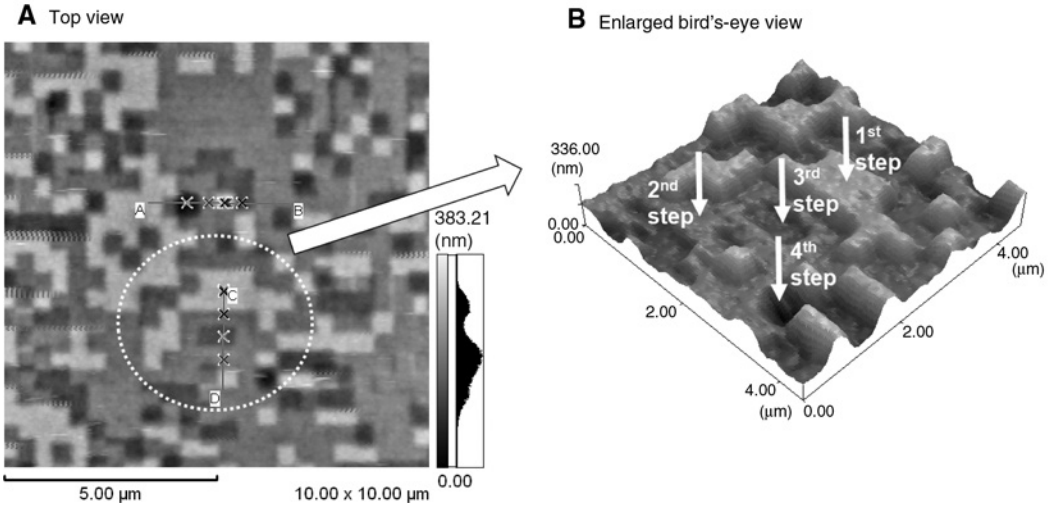

Figure 19: A part of a CGH-ROM pattern obtained by EBL on an SOG with the PEB process.

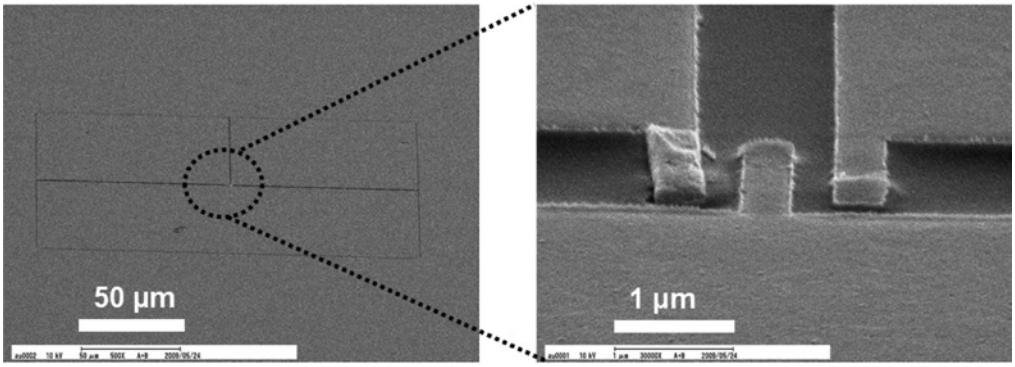

Figure 20: 3D metal electrode pattern obtained by CAV-EBL and nTP of the split metal layer.

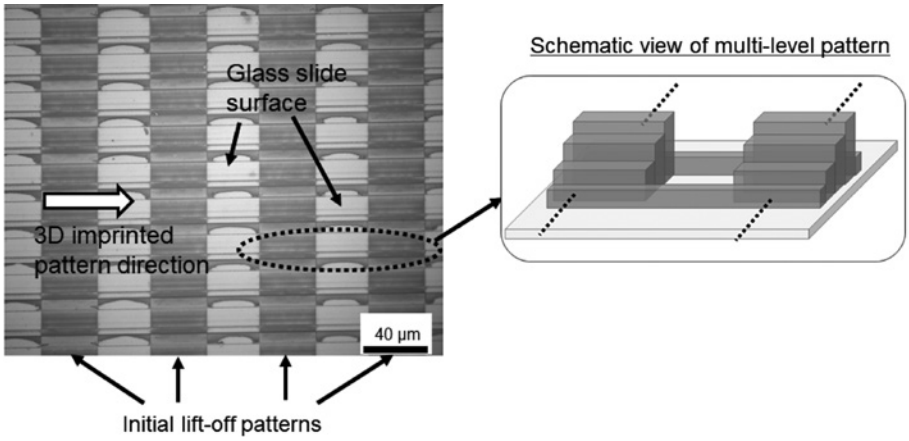

Figure 21: Multilevel calibration plate for TIRFM fabricated by T-NIL using a 3D mold. (Note that the contrast of image was enhanced.)

thickness under the imprinted pattern. When the lift-off pattern and 3D mold are prepared, it is possible to obtain multilevel calibration plates for TIRFM. Figure 21 shows the fabricated multilevel calibration plate for TIRFM. First, line patterns made of MEXFLON [80], the refractive index of which matches that of water, are obtained by the lift-off process. A 3D nanoimprint mold fabricated by CAV-EBL is then used to perform the T-NIL process. At this time, the bottom part of the 3D mold is not contacted to the lift-off pattern because the height of the lift-off pattern is lower than the depth of the 3D mold. As a result, the contacted part is only flowed out, and the 3D MEXFLON patterns on the uncovered area are obtained. The fabrication process and the calibration performance have been reported in detail previously [81–83].

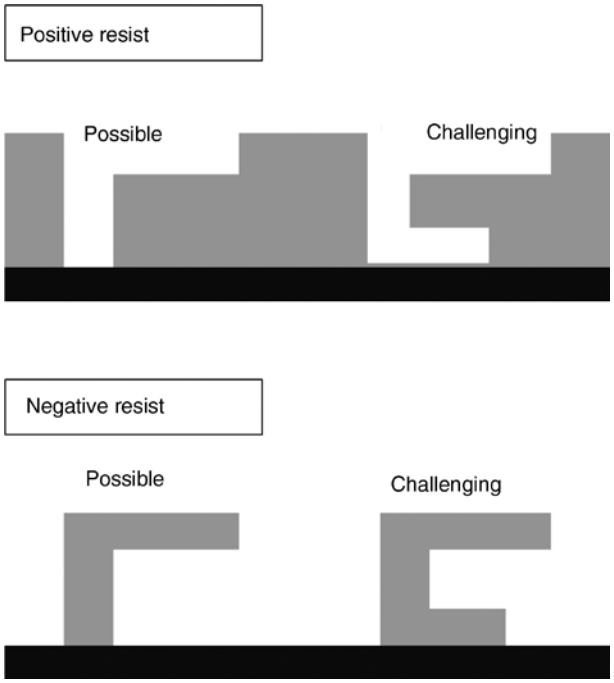

Figure 22: Restriction of the design of developed pattern using CAV-EBL.

5 Summary

3D nanostructures are strongly desired in fabricating and improving next-generation devices in various fields,

such as electronics, optics, biotics, and thermal and fluid dynamics. Although conventional techniques are also useful in fabricating 3D nanostructures, the combination of CAV-EBL with nanoimprinting technology can accelerate 3D fabrications with low cost and high throughput. However, CAV-EBL has some weak points, e.g. the fabrication of multilayered structures (Figure 22) is very difficult because it is impossible to expose at different depth levels in one shot because of the continuous absorption of electrons in the material. However, the nTP process using a 3D mold would be used to stack the imprinted patterns [84, 85]. The design flexibility of 3D nanostructures will be widely expanded using this technique; thus, the nanoimprinting technology using 3D nanostructured molds obtained by CAV-EBL can be used in next-generation 3D nanofabrication.

References

[1] International Roadmap for Devices and Systems, 2017 Edition, Lithography.
[2] C. K. Hu and J. M. E. Harper, Mater. Chem. Phys. 52, 5 (1998).
[3] N. Samoto, Y. Makino, K. Onda, E. Mizuki and T. Itoh, J. Vac. Sci. Technol. B 8, 1335 (1990).
[4] E. Y. Chang, K. C. Lin, E. H. Liu, C. Y. Chang, T. H. Chen, et al., IEEE Electr. Device Lett. 15, 277 (1994).
[5] A. S. Wakita, C.-Y. Su, H. Rohdin, H.-Y. Liu, A. Lee, et al., J. Vac. Sci. Technol. B 13, 2725 (1995).
[6] Y. Chen, D. Macintyre and S. Thoms, J. Vac. Sci. Technol. B 17, 2507 (1999).
[7] Y. Anda, T. Matsuno, M. Tanabe, T. Uda, M. Yanagihara, et al., J. Vac. Sci. Technol. B 17, 320 (1999).
[8] A. Endoh, Y. Yamashita, K. Shinohara, M. Higashiwaki, K. Hikosaka, et al., Jpn. J. Appl. Phys. 41.2S, 1094 (2002).
[9] Y. Chen, D. S. Macintyre, X. Cao, E. Boyd, D. Moran, et al., J. Vac. Sci. Technol. B 21, 3012 (2003).
[10] Y. Chen, Microelectron. Eng. 135, 57 (2015).
[11] P. B. Clapham and M. C. Hutley, Nature 244, 281 (1973).
[12] G. Tricoles, Appl. Opt. 26, 4351 (1987).
[13] S. Noda, K. Tomoda, N. Yamamoto and A. Chutinan, Science 289, 604 (2000).
[14] A. Marmur, Langmuir 20, 3517 (2004).
[15] Y. T. Cheng, D. E. Rodak, C. A. Wong and C. A. Hayden, Nanotechnology 17, 1359 (2006).
[16] P. Kim, T.-S. Wong, J. Alvarenga, M. J. Kreder, W. E. Adorno-Martinez, et al., ACS Nano 6, 6569 (2012).
[17] E. P. Ivanova, J. Hasan, H. K. Webb, V. K. Truong, G. S. Watson, et al., Small 8, 2489 (2012).
[18] C. M. Bhadra, V. K. Truong, V. T. Pham, M. Al Kobaisi, G. Seniutinas, et al., Sci. Rep. 5, 16817 (2015).
[19] L. Feng, Y. Zhang, J. Xi, Y. Zhu, N. Wang, et al., Langmuir 24, 4114 (2008).
[20] Y. C. Tung, Analyst 136, 473 (2011).
[21] Y. W. Lu and S. G. Kandlikar, Heat Transfer Eng. 32, 827–842 (2011).
[22] G. D. Bixler and B. Bhushan, Soft Matter 9, 1620–1635 (2013).
[23] M. Deubel, G. von Freymann, M. Wegener, S. Pereira, K. Busch, et al., Nat. Mater. 3, 444 (2004).
[24] B. Wagner, H. J. Quenzer, W. Henke, W. Hoppe and W. Pilz, Sens. Actuators A: Phys. 46, 89–94 (1995).
[25] C. M. Waits, B. Morgan, M. Kastantin and R. Ghodss, Sens. Actuators A: Phys. 119, 245–253 (2005).
[26] T. Hayashi, T. Shibata, T. Kawashima, E. Makino, T. Mineta, et al., Sens. Actuators A: Phys. 144, 381–388 (2008).
[27] J. Fischer, G. von Freymann and M. Wegener, Adv. Mater. 22, 3578–3582 (2010).
[28] W. Chen and H. Ahmed, Appl. Phys. Lett. 62, 1499–1501 (1993).
[29] D. Winstona, B. M. Cord, B. Ming, D. C. Bell, W. F. DiNatale, et al., J. Vac. Sci. Technol. B 27, 2702–2706 (2009).
[30] M. Kalus, M. Frey, L.-M. Buchmann, K. Reimer and B. Wagner, Microelectron. Eng. 41, 461–464 (1998).
[31] G. Piaszenski, U. Barth, A. Rudzinski, A. Rampe, A. Fuchs, et al., Microelectron. Eng. 84, 945–948 (2007).
[32] K. H. Müller, Phys. Rev. B 35, 7906 (1987).
[33] H. W. P. Koops, R. Weiel, D. P. Kern and T. H. Baum, J. Vac. Sci. Technol. B 6, 477–481 (1988).
[34] Y. Hirai, S. Harada, H. Kikuta and Y. Tanaka, J. Vac. Sci. Technol. B 20, 2867–2871 (2002).
[35] R. Murali, D. K. Brown, K. P. Martin and J. D. Meindl, J. Vac. Sci. Technol. B 24, 2936–2939 (2006).
[36] J. Taniguchi, M. Iida, T. Miyazawa, I. Miyamoto and K. Shinoda, Appl. Surf. Sci. 238, 324–330 (2004).
[37] N. Unno, J. Taniguchi and Y. Ishii, J. Vac. Sci. Technol. B 25, 2361–2364 (2007).
[38] Y. Ishii and J. Taniguchi, Microelectron. Eng. 84, 912–915 (2007).
[39] C. Feldman, Phys. Rev. 117, 455 (1960).
[40] Y. Matsubara, J. Taniguchi and I. Miyamoto, Jpn. J. Appl. Phys. 45, 5538 (2006).
[41] J. Taniguchi, K. Machinaga, N. Unno and N. Sakai, Microelectron. Eng. 86, 676–680 (2009).
[42] K. Osari, N. Unno, J. Taniguchi, K.-i. Machinaga, T. Ohsaki, et al., Microelectron. Eng. 87, 918–921 (2010).
[43] A. del Campo and G. Christian, J. Micromech. Microeng. 17, R81 (2007).
[44] V. Kudryashov, X. C. Yuan, W. C. Cheong and K. Radhakrishnan., Microelectron. Eng. 67, 306–311 (2003).
[45] T. H. P. Chang, J. Vac. Sci. Technol. 12, 1271–1275 (1975).
[46] S. A. Rishton and D. P. Kern, J. Vac. Sci. Technol. B 5, 135–141 (1987).
[47] A. Olkhovets and H. G. Craighead, J. Vac. Sci. Technol. B 17, 1366–1370 (1999).
[48] K. Ogino, J. Taniguchi, S. Satake, K. Yamamoto, Y. Ishii, et al., Microelectron. Eng. 84, 1071–1074 (2007).
[49] N. Unno, J. Taniguchi, M. Shizuno and K. Ishikawa, J. Vac. Sci. Technol. B 26, 2390–2393 (2008).
[50] N. Unno, J. Taniguchi and K. Ishikawa, J. Vac. Sci. Technol. B 29, 06FC06 (2011).
[51] M. Shizuno, J. Taniguchi, K. Ogino and K. Ishikawa, J. Nanosci. Nanotechnol. 9, 562–566 (2009).
[52] H. Miyoshi and J. Taniguchi, Microelectron. Eng. 143, 48–54 (2015).
[53] S. Y. Chou, P. R. Krauss and P. J. Renstrom, J. Vac. Sci. Technol. B 14, 4129–4133 (1996).
[54] J. Haisma, M. Verheijen, K. Van Den Heuvel and J. Van Den Berg, J. Vac. Sci. Technol. B 14, 4124–4128 (1996).

[55] N. Kehagias, V. Reboud, G. Chansin, M. Zelsmann, C. Jeppesen, et al., J. Vac. Sci. Technol. B 24, 3002–3005 (2006).
[56] N. Kehagias, V. Reboud, G. Chansin, M. Zelsmann, C. Jeppesen, et al., Nanotechnology 18, 175303 (2007).
[57] S. Y. Yew, T. S. Kustandi, H. Y. Low, J. H. Teng, Y. J. Liu, et al., Microelectron. Eng. 88, 2946–2950 (2011).
[58] H.-J. Choi, S. Choo, J.-H. Shin, K.-I. Kim and H. Lee, J. Phys. Chem. C 117, 24354–24359 (2013).
[59] K.-S. Han, S.-H. Hong, K.-I. Kim, J.-Y. Cho, K.-w. Choi, et al., Nanotechnology 24, 045304 (2013).
[60] N. Kooy, K. Mohamed, L. T. Pin and O. S. Guan, Nanoscale Res. Lett. 9, 320 (2014).
[61] J. Taniguchi and M. Aratani, J. Vac. Sci. Technol. B 27, 2841–2845 (2009).
[62] J. Taniguchi, S. Tsuji and M. Aratani, J. Vac. Sci. Technol. B 28, C6M45–C6M49 (2010).
[63] H. Maruyama, N. Unno and J. Taniguchi, Microelectron. Eng. 97, 113–116 (2012).
[64] J. Taniguchi, N. Unno and H. Maruyama, J. Vac. Sci. Technol. B 29, 06FC08 (2011).
[65] M. A. Meitl, Z. T. Zhu, V. Kumar, K. J. Lee, X. Feng, et al., Nat. Mater. 5, 33 (2006).
[66] J. Taniguchi, S. Ide, N. Unno and H. Sakaguchi, Microelectron. Eng. 86, 590–595 (2009).
[67] J. Zaumseil, M. A. Meitl, J. W. P. Hsu, B. R. Acharya, K. W. Baldwin, et al., Nano Lett. 3, 1223–1227 (2003).
[68] R. D. Nagel, T. Haeberle, M. Schmidt and G. Scarpa, Nanoscale Res. Lett. 11, 143 (2016).
[69] N. Unno and J. Taniguchi, J. Adv. Mech. Des. Syst. 4, 1022–1032 (2010).
[70] N. Unno, J. Taniguchi, S. Ide, S. Ishikawa, and Y. Ootsuka, et al., J. Phys. Conf. Ser. 191, 012014 (2009).
[71] R. Wakamatsu and J. Taniguchi, Microelectron. Eng. 123, 94–99 (2014).
[72] N. Unno and J. Taniguchi, Microelectron. Eng. 87, 1019–1023 (2010).
[73] N. Unno, S. Yoshida, H. Akamatsu, M. Yamamoto, S.-i. Satake, et al., J. Vac. Sci. Technol. B 31, 06FB01 (2013).
[74] K. Ogino, N. Unno, S. Yoshida, M. Yamamoto and J. Taniguchi, Microelectron. Eng. 123, 163–166 (2014).
[75] Y. Shinonaga, K. Ogino, N. Unno, S. Yoshida, M. Yamamoto, et al., Microelectron. Eng. 141, 102–106 (2015).
[76] N. Unno, J. Taniguchi and S. Ide, J. Vac. Sci. Technol. B 28, C6M32–C6M36 (2010).
[77] N. Unno and J. Taniguchi, Microelectron. Eng. 88, 2149–2153 (2011).
[78] C. Zettner and M. Yoda, Exp. Fluids 34, 115–121 (2003).
[79] H. F. Li and M. Yoda, Meas. Sci. Technol. 19, 075402 (2008).
[80] S. Someya, D. Ochi, Y. Li, K. Tominaga, K. Ishii, et al., Appl. Phys. B 99, 325–332 (2010).
[81] N. Unno, A. Maeda, S. Satake, T. Tsuji and J. Taniguchi, Microelectron. Eng. 133, 98–103 (2015).
[82] N. Unno, S. Nakata, S. Satake and J. Taniguchi, Exp. Fluids 57, 120 (2016).
[83] S. Nakata, N. Unno, S. Satake and J. Taniguchi, Microelectron. Eng. 160, 81–86 (2016).
[84] X. D. Huang, L.-R. Bao, X. Cheng, L. J. Guo, S. W. Panga, et al., J. Vac. Sci. Technol. B 20, 2872–2876 (2002).
[85] T. Tsuji and J. Taniguchi, Microelectron. Eng. 141, 117–121 (2015).